JOURNAL OF MATERIALS SCIENCE **38** (2003) 541 – 547

Effect of composition on phase morphology and mechanical properties of PP/PA66 *in situ* composites via extrusion-drawing-injection method

WEN-YI HUANG, JING-WEI SHEN*, XIAO-MEI CHEN
College of Polymer Science and Engineering, Sichuan University, Chengdu, 610065, Sichuan, People's Republic of China
E-mail: shenjw@stuscu.edu.cn

The reinforced and toughened PP/PA66 *in situ* composites were prepared via extrusion-drawing-injection method. The relationship among composition, phase morphology and mechanical properties, together with their functional mechanism, was investigated. The results show that in the range of PA66 weight fraction (f_w) from 0 to 20% and under the experimental processing conditions, the main changes in phase morphology of the composites with f_w are that the number of *in situ* formed PA66 microfibers and remained PA66 particles increases with f_w whereas the fiber transverse size and its dispersity decrease till $f_w = 15\%$ and then increase. This can be attributed to the combined effect of break-up, coalescence and deformation of the PA66 phase in the PP phase in the course of extrusion and drawing. The tensile strength of composites has a maximum value at f_w of 15% and Young's modulus increases with f_w up to a plateau level, while impact strength continuously rises with f_w, an effect which can be ascribed to the distinct dependence of these properties on the phase-morphological factors mentioned above.

1. Introduction

Since the concept of "*in situ* composites" (ISC) was brought forward more than ten years ago [1]; thermoplastic (TP)/thermotropic liquid polymer (TLCP) composites have been extensively investigated, because several important features of TLCP rigid molecular chains, including easy orientation and fiberization in the flow fields, difficulty to relax as well as high strength and modulus, are potential for performing as a significant reinforcement of the TP matrix. Unfortunately, some demerits of TLCP such as very high price and few species commercially available have become a pronounced impediment in their utilization [2].

However, recent researches indicate that like TLCP, the deformable minor phase composed of flexible-chain TP in some immiscible TP/TP blends under preferential conditions can also achieve similar *in situ* fiberized morphology and in turn has reinforcing and/or toughening effects on the matrix. For example, the reinforced PA6/PA66, PA6/PET ISC, so-called microfibrillar reinforced composites have been prepared through extrusion, post-drawing and then annealing [3, 4], and the toughened PP/PA6 and PP/PET ISC have been obtained by means of extrusion-drawing-compression [5–7].

By comparing with both TP/macro-fiber (e.g. glass fiber) composites and TP/TLCP ISC, the TP/TP ISC are provided with many advantages such as light weight, excellent processability, little abrasion to processing machines and high performance/price ratio, etc. Because of this, the study of their fundamental theory and application possibility has been a topic of growing interest.

In this work, we attempt to prepare the reinforced and toughened PP/PA66 *in situ* composites through single-screw extrusion, melt-drawing with a take-up device, quenching in cool water and then injection moulding at a temperature between the melting points of PP and PA66. In this paper, the phase morphology and mechanical properties of PP/PA66 ISC as a function of varying compositions ($\leq$20 wt%) and their functional mechanisms have been examined by contrast with normal blends without drawing.

2. Experimental

2.1. Materials

Both polypropylene (PP) and polyamide 66 (PA66) are commercially available. The filament-grade PP (F401) with melt index of 2.35 g/10 min was obtained from

*Author to whom all correspondence should be addressed.

Langang Petrochemical Co. Ltd. (China). The PA66 (Y1227) with relative viscosity of 2.67 was obtained from Pingdingshan Shenma Co. Ltd. (China). Within a shear rate ranging from 50 to 500 s^{-1}, the viscosity ratio of PA66 to PP at 270°C was tested to be 0.13–0.47 on a capillary rheometer, an auxiliary of an AG-10TA material testing machine made in Japan.

2.2. Sample preparation

The vaccum-dried PA66 and PP were mixed according to the experimental composition (0–20%PA66 by weight), then melt-extruded on a single-screw extruder of Haake-40 torque rheometer at a fixed screw speed of 25 rpm. The die used was a capillary die with a diameter of 1.59 mm. The temperature profiles of barrel/die were 170–250–275/270°C. For preparing *in situ* composite (ISC) samples, the extrudate was continuously and steadily drawn by adjusting the matched take-up device into a filament with a diameter of 0.62 mm averaged from five measurements and a draw ratio of 6.6 measured by a ratio of cross area of die hole to that of a filament, then quenched in water. With regard to the normal blended (NB) samples, the extrudate did not experience drawing and was cooled in the air into a round strip with a diameter of about 1.6 mm. The filament or strip was granulated, followed by vaccum-drying and subsequently injection moulding into standard bars in the PS40E 5ASE injection machine made in Japan. The temperature profiles of barrel/nozzle for preparing ISC and NB samples are 170–190–210/205°C and 190–250–275/275°C respectively, while other processing parameters are almost identical.

2.3. SEM observations

The JSE-5900LV and AMRAY 1845FM Scanning Electron Microscopes (SEM) were employed for observing the morphology of the following samples: (a) the longitudinal microtoming of a filament and the impact-ruptured surface of an injection bar, in which the PA66 were etched by formic acid; (b) the NB strips, ISC filaments and their corresponding longitudinal sections of injection bars, in which the PP were fully extracted by xylene; (c) the cryogenically fractured surfaces and the impact-ruptured surfaces etched by xylene of NB and ISC injection bars. The all surfaces to be observed were coated with gold under vacuum.

2.4. Mechanical testing

Tensile strength and modulus tests were conducted on an AG-10TA universal material testing machine made in Japan, at the cross-head speeds of 50 and 5 $mm \cdot min^{-1}$ respectively, according to GB/T 1040-92 (China standard). The notched impact strength tests were performed on a UJ-40 izod impact tester made in China, in accordance to GB/T 1843-89 (China standard).

3. Results and discussion

3.1. Phase morphology

Fig. 1 shows SEM micrographs of longitudinal microtoming of a filament and impact-ruptured surface of an injection bar, etched by formic acid, for PP/PA66 (85/15) composites. Fig. 1a combined with Fig. 4c indicates that both PP and PA66 are fiberized in the drawn extrudate, which is similar to the composites obtained from melt spinning of PP/PA6 blends [8]. Fig. 1b combined with Fig. 3b illustrates that the resulting PA66 fibers can be maintained in the injection bars, but PP fibers no longer exist, which melt and relax into an isotropic matrix during injection moulding. Thus, it can be concluded that the preparation of PP/PA66 *in situ* composites was carried out actually through two steps: fiberization of dispersed phase and combination of fibers with matrix, which resembles the course of adding macro-fibers such as glass fiber into polymer matrix. It is evident that this is different from the one-step preparation of TP/TLCP ISC [1, 2].

Figs 2 and 3 show the morphologies of PA66 dispersed phase in the normal blended (NB) and *in situ* composite (ISC) samples respectively, where PA66 contents (f_w) are 15% or 20%. In the NB extrusion and injection samples, PA66 exists always in the form of

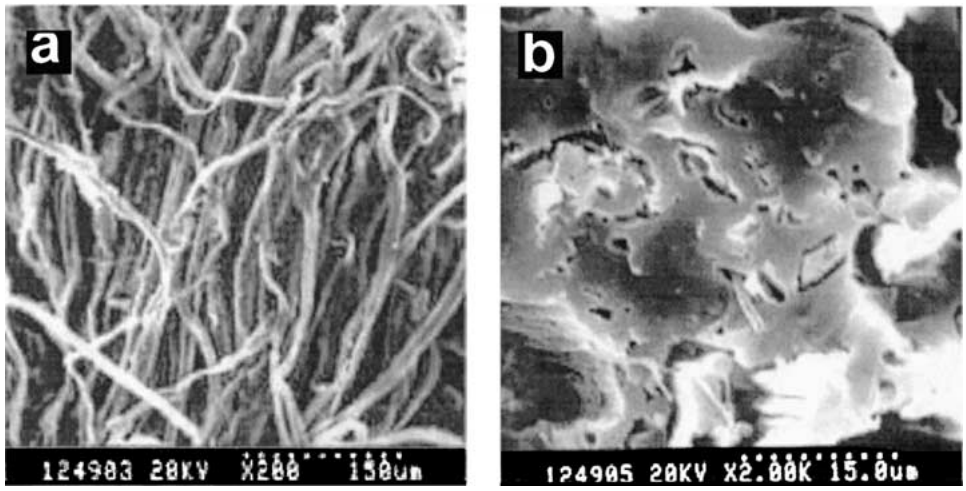

Figure 1 SEM micrographs of PP/PA66 (85/15) composite samples (PA66 was etched by formic acid) (a) longitudinal microtoming of filament, (b) impact-ruptured surface of injection bar.

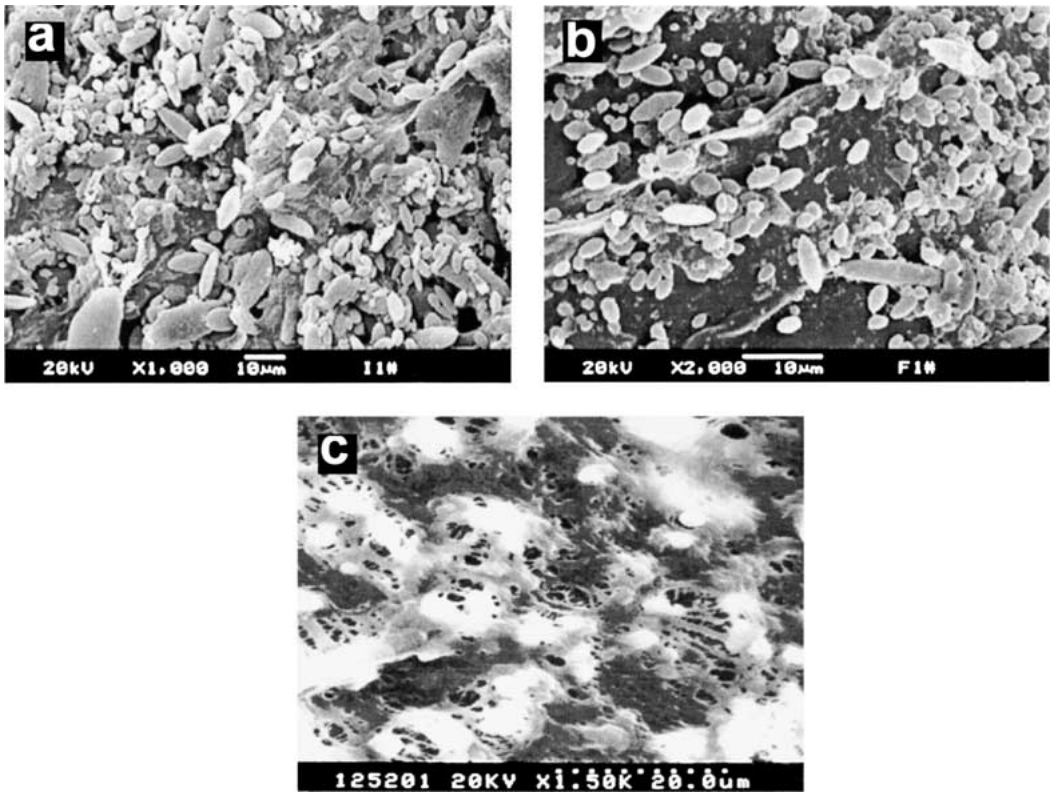

Figure 2 SEM micrographs of PP/PA66 normal blending samples (extracted or etched by xylene) (a) extrudate ($C_d = 15\%$), (b) longitudinal sect-section of injection bar ($C_d = 15\%$), (c) impact-ruptured surface of injection bar ($C_d = 20\%$).

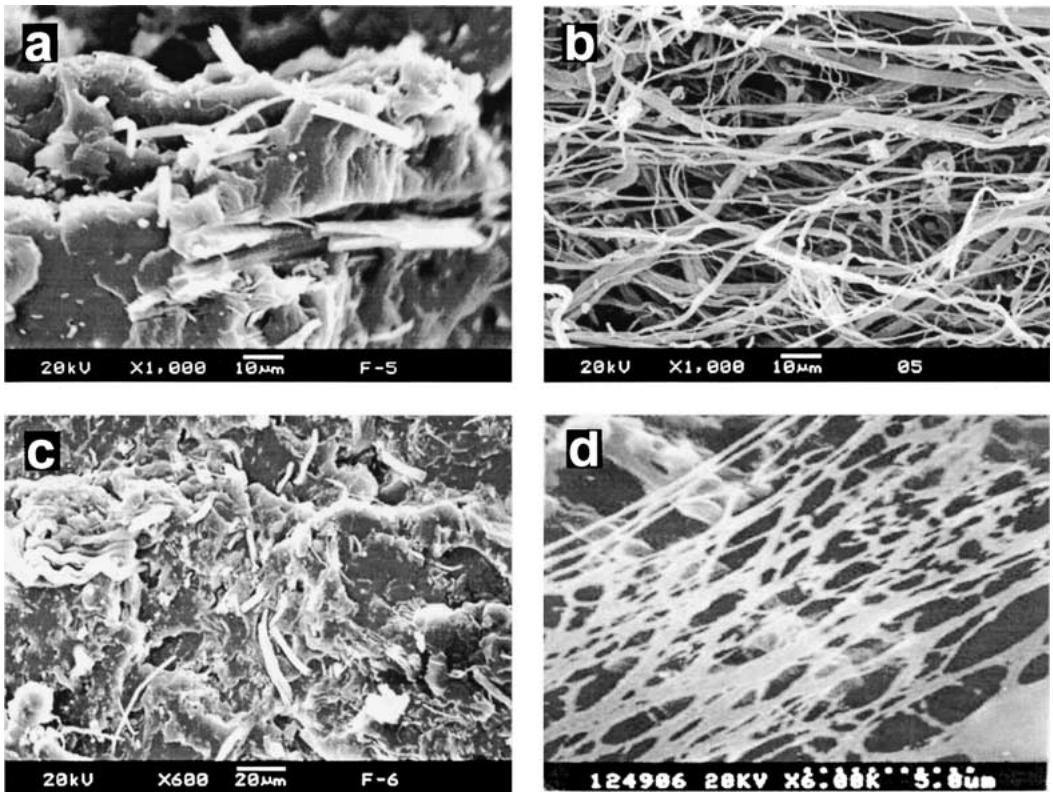

Figure 3 SEM micrographs of injetion samples of PP/PA66 *in situ* composites (a) cryogenically fractured surface ($f_w = 15\%$), (b) longitudinal sect-section ($f_w = 15\%$, extracted by xylene), (c) cryogenically fractured surface ($f_w = 20\%$), (d) impact-ruptured surface ($f_w = 20\%$, etched by xylene).

particles, which can deform to some extent. The particle size ranges from less than 1 μm to more than 10 μm. In the ISC injection samples, PA66 is largely present in the form of fibers, whose diameter or width also has dispersity, ranging from less than 1 μm to several μm. These fibers can entangle with each other to form a fiber network. Meanwhile, there also exist some PA66 particles. This indicates that under the given experimental

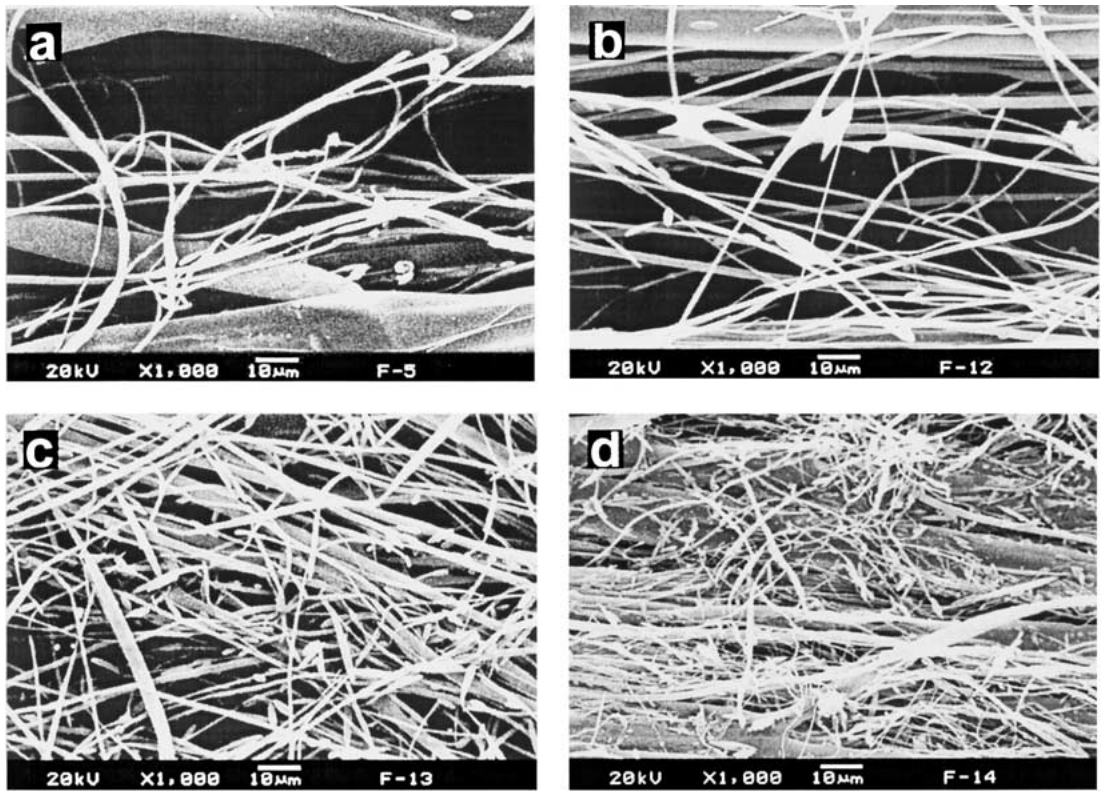

Figure 4 SEM micrographs of PP/PA66 extrusion-drawn filaments with different compositions (PP was fully extracted by xylene) (a) 95/5 (b) 90/10 (c) 85/15 (d) 80/20.

conditions, the PA66 phase in the extruded melt exists in the form of droplets with size dispersity. Under the shearing and limited extensional (existing in the entrance of die) actions in the extruder, the larger droplets can deform to a certain degree but do not fiberize. The droplet-fiber transition of PA66 phase can be accomplished only by means of melt-drawing. The transverse size of the resulting fibers also has dispersity and the degree of droplet-fiber transition are not complete.

Fig. 4 represents the variation of PA66 phase morphology with its contents (f_w) for the ISC filaments, in which the PP was fully extracted by xylene. The results illustrate that (a) PA66 can fiberize even at low concentration of $f_w = 5\%$ and the number of fibers rises with f_w. (b) The transverse size (S_t) of fibers has dispersity, which decreases with f_w when $f_w \leq 15\%$ but becomes larger at f_w of 20%. This can be seem from the change of S_t of the large-end size (coarse) fibers with f_w: when f_w increases from 5% to 15%, the S_t diminishes from more than 10 μm to 4–5 μm, and then increases up to about 8 μm at f_w of 20%. The better uniformity of fibers at $f_w = 15\%$ differs evidently from the unevenness of fibers at $f_w = 20\%$. These are not consistent with the results described in the literature [5–7] that S_t either increases or remains almost unchanged with f_w. (c) There persists PA66 particles in all cases of f_w and their number shows a climbing trend with f_w, as is not pointed out in the literature [5–7].

During the polymer melt blending, the dispersed phase is subjected to two actions of breakup and coalescence. The former is the result of droplet deformation arising from the viscous drag force exerted on the droplets by the matrix exceeding the interfacial tension between two phases, while the latter results from the impingement of droplets due to the intrinsic normal force of viscoelastic droplets. The deformation and breakup of the dispersed droplets are dictated by two parameters [9]: the viscosity ratio of dispersed phase to matrix, $R_V = \eta_d/\eta_m$, and the so-called Weber number, $N_W = r\eta_m\gamma/\sigma = r\tau/\sigma$, where r is radius of droplet, γ shear rate, τ shear stress and σ interfacial tension. When R_V resides in an appropriate range and N_W surmounts a certain critical value, droplets can deform and break up, but it is not the case otherwise. The collision and coalescence of droplets is closely related to the dispersed phase concentration (f_w), and the coalescence can be negligible if f_w is less than 1% [10]. Ultimately, the size and number of droplets are relied on the combined effect of the breakup and coalescence of droplets, which in turn leads to the dispersity of droplet size (Fig. 2).

The previous work of Favis *et al.* [11, 12] concerning the relationship among the number average diameter (d_n) and volume average diameter (d_v), polydispersity (d_v/d_n) and the volume content (ϕ) of the dispersed phase in the about 20 groups of three-pair (including PP-PA6) immiscible polymer blend melts with different R_v and τ/σ has elucidated that d_n, d_v and d_v/d_n all increase with ϕ, and that these d_n (or d_v) and ϕ data are well superimposed on a master curve of d_n (or d_v) plotted against $\phi + \phi^2$. This makes out that ϕ plays a decisive role in the droplet diameter, so that the influences of R_v, σ and τ on the breakup, coalescence and the final diameter of droplets are essentially counterbalanced [11]. The above results that droplet size and its dispersity rise with ϕ or f_w serve as an important basis for the following discussions.

When the extruded melt of an immiscible polymer blend is uniaxially drawn, the larger droplets in the melt will elongate into fibers directly, whereas the smaller droplets will collide and coalesce into larger droplets owing to the intensified interactions between droplets in the course of the contraction of melt transverse section, and in turn extend into fibers. Quantitative analysis can be made to evaluate the relative contribution of these two fiberized mechanisms to the droplet-fiber transition [10]. Since the droplet size and its dispersity in extruded melt increase with f_w, the number of fibers elongately formed both directly from the virgin droplets and from the coalesced droplets will increase with f_w, and the proportion of the latter in the total fiberization also elevates correspondingly [13, 14]. This is the main reason why the dispersed phase can fiberize even at low f_w (e.g. 5%) and the number of fibers increases with f_w (Fig. 4).

Given the constant draw ratio, the transverse size (S_t) of the resulting fibers would depend on both the diameter (d_0) of virgin droplet capable of extending directly into fibers and the diameter (d_c) of coalesced droplet capable of extending into fibers through the coalescence. The alteration of S_t with f_w is then determined by the combined result of the corresponding changes of d_0 and d_c. Since the virgin droplet diameter and its dispersity rise with f_w, d_0 and its dispersity will correspondingly increase, which will result in the increment of S_t and its dispersity. That is to say, the fibers elongately formed from virgin droplets will become coarser and more uneven. Conversely, since the coalescence of droplets during drawing has a function of merging the small droplets and homogenizing the droplet size, and this function enhances with f_w, the diameter dispersity of coalesced droplets and the d_c dispersity will decrease with f_w. Provided that the alteration of d_c with f_w has three possibilities of reduction, invariance and increment, they would result in the reduction, invariance or increment of S_t, respectively. That is to say, as f_w increases, the fibers elongately formed from coalesced droplets may probably become finer, unchanged or coarser, but they would tend to be uniform in all cases. Thus, in case of d_0, d_c and their dispersities changing inversely with f_w, the S_t and its dispersity may reduce (fibers become finer and more uniform) within the range of lower f_w (e.g. $\leq$15%), due to the dominant role of the decrease of d_c and its dispersity with f_w; but at high f_w (e.g. 20%), because the effect of the increase of d_0 and its dispersity becomes pronounced, the S_t and its dispersity may rise (the fibers become coarser and more uneven). This is just the result in Fig. 3. However, if d_c increases or becomes unchanged with f_w, the S_t of the fibers obtained from the two fiberized mechanisms would increase with f_w, which is the result reported in the literature [7]. Only if $d_0 \approx d_c$, they are nearly independent of f_w and their dispersities are very small, the S_t would remain almost invariable without dispersity, as reported in the literature [5, 6].

In the virgin or coalesced droplets, only the larger ones with the diameters of d_0 or d_c can extend into fibers, whereas the smaller ones will be maintained in the filament in the shape of particles or deformed particles. The occurrence probability of these particles increases with f_w because of the raised number of droplets. In addition, the fibers (liquid streams) formed might exhibit capillary wave (varicosity) phenomena on account of the hydrodynamic disturbance arising from the fluctuation of melt density and viscosity or the vibration of the equipment [9]. If the amplitude of such waves equals the radius of the fiber, the liquid stream will break up into droplets. The probability of such action will enhance with f_w because of the increased number of fibers. These two reasons can presumably interpret why there always exists PA66 particles in filaments and their number increases with f_w (Fig. 4).

3.2. Mechanical properties

Fig. 5 depicts the tensile strength (σ_t), Young's modulus (E) and impact strength (a_k) of both NB and ISC injection samples plotted against PA66 contents (f_w), respectively. Over the range of f_w from 0 to 20%, whether for NB or ISC samples, the changing features of σ_t, E and a_k with f_w are distinguishable from each other, whereas the relationships between σ_t or E and f_w for these two kinds of samples demonstrate a similar trend. This implies that the functional mechanisms

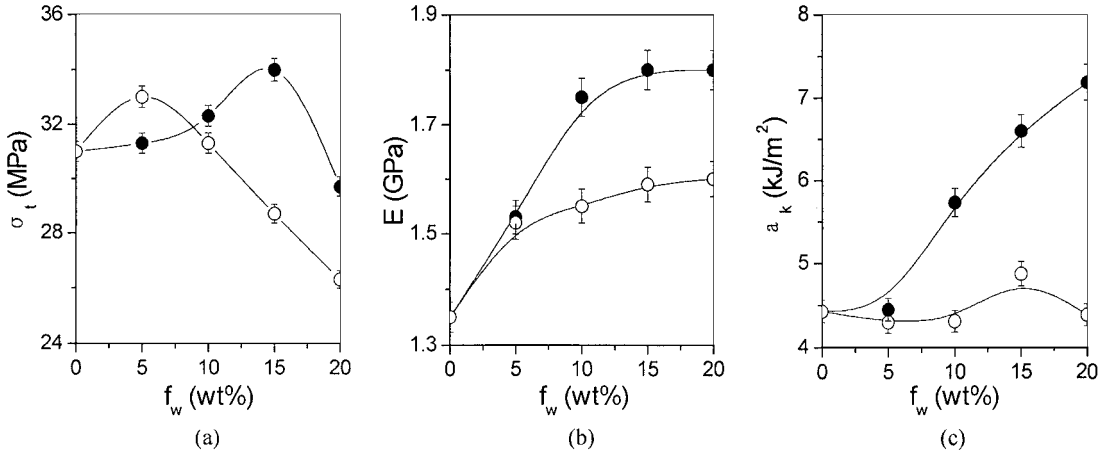

Figure 5 The relationship between the mechanical properties and the PA66 weight fraction (f_w) for two kinds of samples (○ NB ● ISC) (a) Tensile strength (σ_t), (b) Young's modulus (E), (c) Impact strength (a_k).

of f_w influencing these three mechanical properties are substantially different, whereas the structural reasons governing the relationships among σ_t, E and f_w of these two materials are similar.

The σ_t of NB and ISC samples exhibits maximum values at $f_w = 5\%$ and $f_w = 15\%$ (Fig. 5a), respectively. It is assumed that this is the competitive and counterbalanced consequence between the reinforcing effect of the dispersed phase and the interfacial flaw effect of two phases. The former refers to the fact that the dispersed phase, whose bulk strength is superior to that of the matrix, has a reinforcing action on the matrix and the fibers with axial strength exceeding bulk strength have more reinforcing action than particles, and this action will enhance with f_w due to the raised number of particles or fibers. The latter points to the fact that there are voids at the weakly adhesive interface between two phases; during the tensile tests with slow loading, these voids obstruct the transfer of stress from matrix to the dispersed phase, which makes the dispersed phase unable to bear and disperse the loading effectively, and themselves become the stress concentrators and weak sites of material structure, which results in the decrease of failure stress of the materials. This negative effect becomes more noticeable due to the increased size or number of voids with f_w. Over the f_w range with the former effect surpassing the latter one, the σ_t of materials will be promoted, but it is the reverse case otherwise. For NB samples, the reinforcing effect of the dispersed phase (PA66 particles) is weaker in comparison with the stronger interfacial flaw effect (larger size of the voids), so σ_t diminishes when f_w is greater than 5%. With regard to the ISC sample, as the f_w increases in the range of less than 15%, because of the increment of fiber number as well as the decrement of fiber transverse size (S_t) and its dispersity (the finer and more uniform fibers can reduce the interfacial void size), the σ_t increases due to the reinforcing effect of the dispersed phase exceeding the interfacial flaw effect. But at f_w of 20%, because S_t and its dispersity become greater with many coarse fibers and remained particles, in spite of the increased number of fibers, the σ_t falls due to the prominent role of the interfacial flaw effect.

The E–f_w relationship of NB and ISC samples (Fig. 5b) demonstrates that PA66 particles, whose bulk modulus is larger than that of the matrix, have rigidizing action on the PP matrix (its amorphous region is at rubbery state at room temperature), and PA66 fibers with axial modulus exceeding bulk modulus have more rigidizing action than particles. This action will enhance with f_w due to the raised number of PA66 particles or fibers. However, when the distribution density of the particles or fibers in the matrix is sufficiently high, the enhancement of the rigidizing action becomes imperceptible in the range of f_w examined, and then the E of materials arrives at a plateau level.

The impact strength (a_k) of ISC samples continuously increases with f_w while the a_k of NB samples almost remains unchanged (Fig. 5c). The a_k of ISC sample with f_w of 20% is higher by 65% than that of pure PP. This gain of a_k is more apparent than the utmost ones of σ_t (10%) and E (36%). In the high-speed loading impact tests, when the stress transfers from low-modulus matrix to high-modulus fibers, it can be dispersed throughout the whole fibers and spread to a wide region owing to the large ratio of surface to volume of fibers and the formation of fiber network (Figs 3 and 4), which will greatly diminish the effect of stress concentration of voids at the interfaces, and in turn prevent the initiation of crack at the voids and inhibit its propagation as soon as it is initiated, so the impact destruction energy is significantly improved [2]. In addition, when the material is impact-ruptured, the sliding, pullout and breakup of the fibers (Fig. 3a and c) will absorb a large amount of impact energy [15], which also contributes to the increment of a_k. Therefore, as f_w increases, the continuous increment of PA66 fiber number as well as the formation and perfection of fiber network is the structural reason of the continuous enhancement of a_k. However, the above two mechanisms are not present in NB samples, so they can't exhibit the toughening effect. It is because the a_k of ISC samples is mainly controlled by the fiber morphology rather than the interfacial structure that the large gain of a_k can be obtained at high f_w. But for the σ_t, which is restricted always by the interfacial flaw effect, it falls at higher f_w and its utmost gain is also limited. The use of compatibilizer in an appropriate manner can markedly promote the interfacial adhesion and the reinforced effect, without influencing the PA66 fiberizability, as will be reported elsewhere.

4. Conclusions

The reinforced and toughened PP/PA66 *in situ* composites can be prepared via extrusion-drawing-injection moulding method. Under the experimental processing conditions, as the PA66 content (f_w) increases from 0 to 20%, the number of *in situ* formed PA66 fibers rises, and the fiber transverse size and its dispersity decrease till $f_w = 15\%$ and then increase as well as the number of remained PA66 particles also tend to rise. This can be attributed to the combined effect of breakup, coalescence and deformation of the PA66 phase in the PP phase in the course of extrusion and drawing. Correspondingly, the tensile strength (σ_t) of the *in situ* composites increases till $f_w = 15\%$ and then decreases, whereas the Young's modulus (E) increases up to a plateau level and the impact strength (a_k) continuously rises with f_w. This can be ascribed to the distinct dependence of these properties on the phase-morphological factors mentioned above. The σ_t is primarily controlled by the reinforcing effect of the dispersed phase and the interfacial flaw effect of two phases, and it is promoted when the former effect surpasses the latter one and will reduce in the reverse case. The increment of E can be associated with the enhancement of the rigidizing effect of the dispersed phase on the matrix. The continuous increment of a_k results from the raised number of fibers as well as the development of fiber network.

Acknowledgements

The authors gratefully acknowledge the support of Doctoral Research Foundation granted by the National Ministry of Education, China (Grant No. 20010610031).

Special thanks are also due to the State Key Laboratory of Polymer Materials Engineering, Sichuan University for the structural characterizations.

References

1. G. KISS, *Polym. Eng. Sci.* **27** (1987) 410.
2. A. MEHTA and A. I. ISAYEV, *ibid.* **31** (1991) 971.
3. M. EVASTATIEV, J. M. SCHULTZ and S. PETROVICH, *J. Appl. Polym. Sci.* **67** (1998) 723.
4. M. EVASTATIEV, J. M. SCHULTZ, S. FAKIROV *et al.*, *Polym. Eng. Sci.* **41** (2001) 192.
5. X. LI, M. CHEN *et al.*, *Polym. J.* **29** (1997) 975.
6. X. LI, M. CHEN *et al.*, *Polym. Eng. Sci.* **39** (1999) 881.
7. M. CHEN, Y. HUANG, S. ZHAO *et al.*, *Chinese J. Appl. Chem* **12**(6) (1995) 77.
8. B. R. LIANG, J. L. WHITE, J. E. SPRUIELL *et al.*, *J. Appl. Polym. Sci.* **28** (1983) 2011.
9. M. V. TSEBRENKO, G. P. DANILOVA and A. Y. MALKIN, *J. Non-Newton. Fluid Mech.* **31** (1989) 1.
10. R. GONZALEZ-NUNEZ, D. DE KEE and B. D. FAVIS, *Polymer* **37**(21) (1996) 4689.
11. B. D. FAVIS and J. M. WILLIS, *J. Polym. Sci. Part B:Polym. Phys.* **28** (1990) 2259.
12. J. M. WILLIS, V. CALDAS and B. D. FAVIS, *J. Mater. Sci.* **26** (1991) 4742.
13. R. GONZALEZ-NUNEZ, B. D. FAVIS and P. J. CARREAU, *Polym. Eng. Sci.* **33**(13) (1993) 851.
14. N. CHAPLEAU and B. D. FAVIS, *J. Mater. Sci.* **30** (1995) 142.
15. E. D. WILLIAMS, L. S. SCHADLER and A. LUSTIGER, *Ann. Tech. Conf.—ANTEC, Conf. Proc., 1998 Soc. Plast. Eng.* **2** (1998) 2266.

Received 14 December 2001
and accepted 24 September 2002